



**University of
Sunderland**

Chen, Meng, Baglee, David, Chu, Jiang Wei, Du, Danfeng and Guo, Xiurong (2017) Photocatalytic oxidation of NO_x under visible light on asphalt pavement surface. *Journal of Materials in Civil Engineering*, 29 (9). p. 1. ISSN 0899-1561

Downloaded from: <http://sure.sunderland.ac.uk/id/eprint/7100/>

Usage guidelines

Please refer to the usage guidelines at <http://sure.sunderland.ac.uk/policies.html> or alternatively contact sure@sunderland.ac.uk.



**University of
Sunderland**

Chen, Meng, Baglee, David, Chu, Jiang Wei, Du, Danfeng and Guo, Xiurong
(2017) Photocatalytic oxidation of NO_x under visible light on asphalt pavement
surface. *Journal of Materials in Civil Engineering*, 29 (9). ISSN 0899-1561

Downloaded from: <http://sure.sunderland.ac.uk/7100/>

Usage guidelines

Please refer to the usage guidelines at <http://sure.sunderland.ac.uk/policies.html> or alternatively contact sure@sunderland.ac.uk.

1 Photocatalytic oxidation of NO_x under visible light on asphalt pavement surface

2 Meng Chen¹, David.Baglee², Jiang Wei Chu³, Dan feng Du⁴, Xiu rong Guo⁵

3 ¹College of Traffic, Northeast Forestry University, 26 Hexing Road, Xiangfang District, Harbin,
4 150040, P.R. China, E-mail: chenmeng623@126.com

5 ² Faculty of Applied Sciences, University of Sunderland, ST PETERS WAY, Sunderland, SR6
6 ODD, United Kingdom, E-mail: David.Baglee@sunderland.ac.uk

7 ³ College of Traffic, Northeast Forestry University, 26 Hexing Road, Xiangfang District, Harbin,
8 150040, P.R. China, E-mail: wildlife_deer@126.com

9 ⁴ College of Traffic, Northeast Forestry University, 26 Hexing Road, Xiangfang District, Harbin,
10 150040, P.R. China, E-mail: chenyuqi0831@163.com

11 ⁵ College of Mechanical and Electrical engineering, Northeast Forestry University, 26 Hexing
12 Road, Xiangfang District, Harbin, 150040, P.R. China, E-mail: 785199452@qq.com

13 Corresponding author : Xiu rong Guo

14
15 Abstract:

16 This work examines the potential use of heterogeneous photocatalysis as an innovative oxidation
17 technology. The aim is to demonstrate that this technology can reduce the damaging effects of
18 vehicle emissions by using nitrogen doped (N-doped) TiO₂ as a photocatalyst immobilized above
19 the asphalt road surface. In the study, the photocatalytic effectiveness and durability of N-doped
20 TiO₂ photocatalytic asphalt road material were assessed in both the laboratory and the field using
21 direct and indirect measurement. The experimental results show that under visible light irradiation,
22 N-doped TiO₂ asphalt road material has a higher activity compared with pure TiO₂ asphalt road
23 material. The decontamination rate for NO_x is about 27.6%, 24.6%, 16.3%, and 13.8% under

24 irradiation at light wavelengths of 330–420 nm, 430–530 nm, 470–570 nm and 590–680 nm,
25 respectively. Results of the field test and prediction models suggest that the service life of
26 N-doped TiO₂ asphalt road material is approximately 13 months.

27

28 Key word: Photocatalyst; N-doping; visible light; Photocatalytic asphalt pavement; Nitrogen
29 oxides

30

31 Introduction

32 Urban areas experience high levels of traffic exhaust, which contribute to air pollution, which
33 is a major global concern (Ishihara et al. 2010). Many governments have introduced emission
34 reduction systems in order to decrease emissions. In spite of these efforts, traffic has continued
35 to increase, adding to concerns about the influence of traffic emissions on health and the
36 environment. Researchers have found that asthma is associated with nitrogen oxide (NO_x), which
37 pedestrians are exposed to due in part to the proximity of roads to walkways. Motor vehicle
38 emissions must be decreased in order to reduce nitrogen oxide emissions, and thus reduce asthma
39 rates (Tarek Mohamed et al. 2009). There are a number of methods that can be used to eliminate
40 NO_x and other pollutants.

41 Recently, heterogeneous photocatalysis has emerged as an ecological technique for
42 controlling air pollutants. In this technique, TiO₂ and pavement materials (such as cement and
43 asphalt) are used together as a photocatalyst; this method has been found to be a promising and
44 valid technology for NO_x control. The de-polluting properties of TiO₂ photocatalytic materials
45 have been assessed by applying this method both in real-world use and in laboratory simulations

46 performed under different experimental conditions. Pone and Cheung (2006) evaluated the NO
47 removal paving blocks produced by waste materials and TiO₂. Their study included an optimum
48 mix design incorporating recycled sand, glass, 10% TiO₂, and cement achieved 4.01 mgh⁻¹m⁻² NO
49 removal. Husken et al., (2007) performed a comparative analysis of different photocatalytic
50 cementitious products in an optimum laboratory conditions. They found that the efficiency of NO_x
51 degradation varied significantly, with some products achieving 40% degradation while others had
52 no influence. In Bergamo, Italy in 2006 (Guerrini and Peccati. 2007) a 12,000 m² area, was
53 developed on the sidewalk and the road using active paving blocks. Environmental monitoring
54 showed an average NO_x abatement of 45% during the daytime (09:00 -- 17:00).

55 In asphalt roads, based on the porous characteristics of asphalt road materials, Meng Chen et
56 al. (2010) used permeability technology to apply asphalt nano-TiO₂ as an environmental
57 protection material. This test showed that this type of photochemical catalysis environmental
58 protection material had a purification function and the ability to protect the environment. Marwa
59 Hassan et al. (2013) used the pray method to make photocatalytic asphalt pavements. Laboratory
60 evaluation showed that the maximum NO_x removal efficiency was reached at an application rate
61 of 0.05 L/m². A research team in Italy used a mixed method approach to develop environmental
62 protection materials. TiO₂ was added into asphalt pavements as an apparent layer that is sprayed
63 onto existing pavements. The decrease in efficiency was dependent on the type of TiO₂
64 nanoparticles used, and the NO_x decrease efficiency ranged from 20–57% (Venturini et al. 2009).

65 Photocatalytic asphalt pavements mainly use anatase phase TiO₂. The TiO₂ band gap is 3.2eV,
66 which corresponds to wavelengths less than 388 nm. This limits the photocatalytic practice in the
67 UV light region, which amounts to 4% of the solar spectrum, while the key part (45%) falls under

68 the visible light region (Chun-Hung et al. 2010). Few studies have attempted to use photocatalytic
69 asphalt pavements under visible light irradiation. Therefore, this study focuses on making a
70 photocatalytic asphalt pavement material. As an innovative oxidation technology, it is able to
71 reduce the damaging effects of vehicle emissions by using N-doped TiO₂ as a photocatalyst that is
72 immobilized above the asphalt road's surface under visible light irradiation. The decontamination
73 effect and application durability of the photocatalytic asphalt pavement material are also analyzed
74 in this study.

75

76 Experimental

77 Photocatalysts preparation

78 A non-metal doping approach (N-doped TiO₂) was used to extend the utilization of the visible
79 region in the solar spectrum. Titanium powder was prepared using a sol–gel approach that used
80 tetrabutyl titanate (TNBT) and distilled water as the titanium precursor and hydrolyzing agent.
81 First, TNBT was mixed with ethanol and distilled water. Then, the mixed solution was stirred
82 using a machine under an 85 °C temperature bath for 6 hours. The slurry was dried at 80 °C and
83 calcined at 400 °C for one hour. Finally, a white powder was obtained, which was pure TiO₂ (see
84 Figure 1).

85 The pure TiO₂ powder was mixed with urea at molar ratios of 2:1, and then ground in an
86 agate mortar for homogeneity. The mixed powders were heated in a muffle furnace at 500 °C for 3
87 h, resulting in N-doped TiO₂ (Figure 1).

88 Figure 1 shows that the N-doped sample appears yellow in color, compared to the white color
89 of the pure TiO₂. Giacomo Barolo (2012) and Shinri Sato (1986) also observed these differences

90 in color and found that the yellow-colored N-TiO₂ had greater photocatalytic activity.

91 Preparation of asphalt road material through the addition of N-doped TiO₂ nanoparticles

92 We performed a series of penetrating load tests in order to attain a photocatalytic asphalt road
93 material sample. First, based on our preliminary research (Meng and Yan hua. 2010), the penetrant
94 and modified N-doped TiO₂ with silane coupling reagent were prepared. Then, the solution of
95 mixed penetrant and modified N-doped TiO₂ was sprayed onto the bituminous sample's surface. In
96 the load process, every sample was sprayed three times by an atmospheric air compressor. The
97 caliber of the air compressor was 1.5mm and the air pressure was 3.0-3.5MPa. The samples were
98 sprayed at a distance of approximately 20 cm and the speed of the aqueous solution jet was set at
99 8-10g/s.

100 Figure 2 and 3 display the schemes of the asphalt road material sample before and after spraying.

101

102 Analytical methods

103 Material property analytical methods

104 A scanning electron microscopy (SEM), and transmission electron microscopy (TEM) were
105 used in this research in order to analyze the material properties of the N-doped TiO₂ and the
106 photocatalytic asphalt road material. The SEM was a commercial Hitachi S2300 instrument with a
107 tungsten hairpin filament. An accelerating voltage of 25 keV was used on gold samples to
108 eliminate charging. Transmission electron microscopy analyses were performed using a JEM-2010
109 (JEOL) operating at 160 kV. T.

110 Photocatalytic degradation analytical methods

111 Direct and indirect measurement strategies were used in this research to evaluate the
 112 pollutant removal efficiency. Direct measurements were used in laboratory tests. In the laboratory
 113 test, 500 ppb of NO_x was put into the measurement system. After flowing through the
 114 photocatalytic asphalt road material, it was exported via the purification examination photoreactor
 115 of the system. Measurement results of the inlet and outlet of photoreactor show that the total NO_x
 116 concentration, the NO conversion, NO₂ conversion, and NO_x conversion were:

$$117 \quad \text{NO}_x = \text{NO} + \text{NO}_2 \quad (1)$$

$$118 \quad \text{NO}_{\text{conversion}} = \left(\frac{C_{\text{NOin}} - C_{\text{NOlight}}}{C_{\text{NOin}}} - \frac{C_{\text{NObin}} - C_{\text{NOsb}}}{C_{\text{NObin}}} \right) \times 100\% \quad (2)$$

$$119 \quad \text{NO}_{2\text{conversion}} = \left(\frac{C_{\text{NO}_2\text{in}} - C_{\text{NO}_2\text{light}}}{C_{\text{NO}_2\text{in}}} - \frac{C_{\text{NO}_2\text{bin}} - C_{\text{NO}_2\text{sb}}}{C_{\text{NO}_2\text{bin}}} \right) \times 100\% \quad (3)$$

$$120 \quad \text{NO}_{x\text{conversion}} = \left(\frac{C_{\text{NO}_x\text{in}} - C_{\text{NO}_x\text{light}}}{C_{\text{NO}_x\text{in}}} - \frac{C_{\text{NO}_x\text{bin}} - C_{\text{NO}_x\text{sb}}}{C_{\text{NO}_x\text{bin}}} \right) \times 100\% \quad (4)$$

121

122 The parameter meaning of equations 1,2, 3, and 4 are described in table 1.

123 The concentration of nitrates serves as evidence of a photocatalytic decrease of NO_x.
 124 Nitrates that accumulate on the pavement surface were measured by dissolving them in deionized
 125 water. Using the Japanese industrial standard (JIS TR Z 0018 “Photocatalytic materials--- air
 126 purification test procedure”), the nitrogen compound eluted from the test piece was calculated
 127 using the following formula (David et al. 2014):

$$128 \quad Q_w = Q_{w1} + Q_{w2} = V_{w1} [(NO_3^-)_{w1} / 62] + [(NO_3^-)_{w2} / 62] \quad (5)$$

129 where Q_w = nitrogen compound eluted from the test piece (μmol); V_w = volume of collected
 130 washing (mL); NO₃⁻ = nitrate ion centration eluent from the test piece (mg/L); and W₁ and W₂ =
 131 the first and second DI washes, respectively.

132 Experimental testing: testing system and set-up

133 Experimental testing system

134 Photocatalytic degradation of NO_x was carried out using a continuous flow system that
135 included a gas supply subsystem, photoreactor, and the analytic subsystem. NO_x , N_2 , and
136 humidified air were supplied in the gas supply subsystem. Humidified air was prepared by
137 bubbling air through a gas wash bottle containing water. The desired water vapor level can be
138 obtained by varying the flow rate of the humidified air stream. To obtain a stable NO_x
139 concentration, NO_x is mixed with humidified air in a gas mixer. During the experiments, gas flow
140 rates are controlled by calibrated flow meters. The photoreactor in the flow system is made of
141 quartz glass in accordance with the American Material Test Association standard (ASTMD
142 5116-1990) and the Japanese industrial standard (photochemical catalysis material-air purification
143 performance test method (Marwa et al. 2010)). To simulate on-road automobile exhaust, the
144 photoreactor is divided into three parts (1) an inlet, (2) purification region and (3) outlet. The inlet
145 section is nearly a cylinder; a fan controls the stream gas velocity. The purification section is
146 rectangular, which simulates the road surface. Humidity and temperature sensors and a heater
147 were installed in the photoreactor, and the photoreactor was irradiated by a simulation light source.
148 Figure 4 shows the entire photoreactor structure. In the analytic subsystem, NO , NO_2 , and NO_x
149 concentration is measured by the analyzer.

150

151 Testing set-up

152 Photocatalytic activity rests: Previous studies on photocatalytic asphalt roads have shown that
153 illumination by a light source is an essential condition for photodegradation of NO_x . Light source

154 illumination can cause the formation of electron–hole pairs on the photocatalytic asphalt road
155 material and the electron–hole pair purified NO_x (Meng and Yan hua. 2010). In this study, we
156 attempt to increase insight into the reduction of NO_x under photocatalytic asphalt road material by
157 looking at the influence of the light source on the process.

158 During the serial experiment, the photocatalytic activity of N-doped TiO₂ photocatalytic
159 asphalt road material was investigated by assessing the NO_x decomposition in the photoreactor.
160 The experiment consisted of three steps.

161 Step 1: the sample was kept in the dark for 40 min, in order to achieve adsorption and desorption
162 equilibrium of NO_x gas in the photoreactor.

163 Step 2: the light source was switched on. The range of the light wavelength is 330–420 nm,
164 430–530 nm (blue LED), 470–570 nm (green LED), and 590–680 nm (red LED).

165 Step 3: Photocatalytic characterizations of samples were shown using different NO_x concentration
166 or decontamination rates. Direct measurement was used throughout the experiment.

167 Tests of application durability: In order to measure long term effects and examine
168 decontamination durability, it is necessary to apply N-doped TiO₂ photocatalytic to asphalt road
169 material to decontaminate exhaust from traffic in an outdoor environment. Vehicular activity and
170 rainwash are major influencing factors in actual outdoor traffic environments.

171 A field and simulation test were adopted in order to predict the durability of the N-doped
172 TiO₂ asphalt road material. In the field test, the test roads were washed once per week. At the same
173 time, traffic volume, temperature, wind direction, wind speed, and humidity were recorded.

174 During the test, the UV–vis spectroscopy (TU-1901) was used to determine absorbency of the
175 gathered sample by N-(1-naphtyl)-cethylncndiaminc dihydrochloride colorimetric (Meng et al.

176 2014). The entire test was executed under nature flow conditions in the daytime and separate
177 specimen exams lasted one hour. The field test location is shown in Figure 5.

178 Two separate simulation tests were conducted. First, in order to study the effect of vehicular
179 activity, the Loaded-Wheel Tester was used to simulate loading and wear on the N-doped TiO₂
180 photocatalytic asphalt road surface (see Figure 6). The photocatalytic activities of samples that
181 were subject to wear were investigated by evaluating the decomposition of NO_x in the
182 photoreactor. The second test studied the rain wash effect. The samples were placed in to a traffic
183 environment from June to August in Harbin, China. After this period a wash test was conducted.
184 The samples were washed once a week and direct and indirect measurements were used to
185 evaluate decontamination ability.

186

187 Results and discussion

188 Physical properties

189 TEM was executed to investigate the micrographs and dispersion of N-doped TiO₂ in the penetrant.
190 Fig.6 shows that the micrographs of the N-doped TiO₂ are spherical and there is no significant
191 shape change. The findings show that urea can help to hold or diminish the mean size and increase
192 the homogeneity of the size distribution via the synthesis method, which has been described by
193 other researchers (Hao-Hong et al. 2013). N-doped TiO₂ was also well dispersed in the penetrant
194 as seen in Figure 8. An integrated method was used to ensure the dispersion effect of N-doped
195 TiO₂ in the penetrant. It included three techniques. One technique used a silane coupling agent as
196 a modifier, which should help N-doped TiO₂ to have good compatibility in the penetration process.
197 Another technique involved choosing a magnetic stirrer for stirring the quantitatively modified

198 N-doped TiO₂. In the third technique, an ultrasonoscope was used to disperse the mixing solution
199 in order to reduce spontaneous reunion and flocculation.

200 The comprehensive dispersion method achieved a good dispersion effect for the following
201 reasons: (1) The affinity between the nanoparticles and the solvent increased; meanwhile, it was
202 easier to open the nano-granular equipment, reducing the dispersion time and energy consumption.
203 (2) The strong turbulent motion of the liquid flow caused by the magnetic stirring broke and
204 suspended the nano-particle and the ultrasonic agitation continued to disperse the nanoparticles
205 into small particles, which led to a wide range of the solution region. (3) In the modifier
206 component, one end of the active groups can be adsorbed on the surface of the crashed
207 nanoparticles and the other end of the solvent formed adsorption layer, which produced electric
208 charge repulsion, guaranteeing long dispersed suspension of the nanoparticles in the solvent,
209 avoiding flocculation and ensuring the stability of the system.

210 Photocatalytic activity and purification mechanism

211 Figure. 9 shows the decontamination ability of the pure TiO₂ asphalt road material and
212 N-doped TiO₂ asphalt road material, where the different wavelength lights (330–420 nm, 430–530
213 nm, 470–570 nm, and 590–680 nm) were irradiated to the samples. As seen in Figure 8, there was
214 no loss of photoactivity in 330–420 nm wavelength lights (including in the UV section) on the
215 pure TiO₂ asphalt road material and N-doped TiO₂ asphalt road material. Meanwhile, the N-doped
216 TiO₂ asphalt road material had NO_x decontamination abilities of about 27.6%, 24.6%, 16.3%, and
217 13.8% under the irradiation of light wavelengths 330–420 nm, 430–530 nm, 470–570 nm, and
218 590–680 nm respectively. Further, on the N-doped TiO₂ asphalt road material under light
219 irradiation, the NO decontamination ability was better than the NO₂ decontamination ability.

220 A number of results can be extracted from Figure 9.

221 (1) N-doped TiO₂ asphalt road materials have better photocatalytic activity under visible light

222 There are two potential reasons for this. First, it is well known that photocatalysts need light
223 illumination to trigger photocatalytic oxidation. Figure 8 shows that the N-doped TiO₂ asphalt
224 road material had better NO_x decontamination ability under a wavelength range of visible light.
225 The N-doped TiO₂ asphalt road material absorbed visible light to trigger photocatalytic oxidation.
226 Second, the behavior of the N-doped TiO₂ asphalt road material in the NO_x oxidation was also
227 associated with the active species ($\bullet\text{OH}$ and $\text{O}_2\bullet^-$) formed on the photocatalyst's surface
228 (Todorova et al. 2013). Excite electrons were required from the valence band to create electron
229 and hole pairs. Equation 6 (Shu et al. 2004) shows that energy decreases from irradiation for
230 exciting surface electrons and holes with increasing wavelength of the visible light. It indicated
231 that the band gap might be significantly narrowed by mechanical chemistry doping of nitrogen in
232 titanium, for instance 3.08 eV (Gagoa et al. 2012).

$$233 \quad E_g = 1239.8 / \lambda \quad (6)$$

234 where E_g is the band gap (eV) of the sample, λ (nm) is the wavelength of the onset of the
235 spectrum.

236 (2) N-doped TiO₂ asphalt road material had different photocatalytic activity under different
237 visible light wavelengths.

238 Figure 9 shows that the activity for the N-doped TiO₂ asphalt road material was clearly better
239 than the pure TiO₂ asphalt road material activity with increasing wavelengths. The findings were
240 attributed to the introduction of N in the TiO₂ lattice and the creation of extra electronic states in
241 the TiO₂ band gap (Kumar et al. 2011).

242 The N-doped TiO₂ samples possessed a two-step adsorption spectra. The first step may have
243 been related to the original titanium band structure and the second adsorption step (in the visible
244 light region) may have been related to the formation of additional electronic states during nitrogen
245 doping (Shu et al. 2008).

246 Figure 8 shows that decontamination of the NO_x ability of the N-doped TiO₂ asphalt road
247 material decreased with increasing wavelength of the light in. The rate of electron and hole pair
248 recombination was a key factor affecting the decontamination NO_x ability of N-doped TiO₂
249 asphalt road material (Yao-Hsuan et al.2011). Photoluminescence emission occurs when
250 wavelength photoenergy is absorbed to excite an electron from the valence band and then a longer
251 wavelength luminescence was emitted via recombination of the electron-hole pair (Chun-Hung et
252 al 2012). The greater the luminescence intensity was, the quicker the electron and hole
253 recombined. Therefore, high intensity of luminescence might result in low photocatalytic activity
254 (Yu et al., 2005). Therefore, the N-doped TiO₂ is capable of lowering the luminescence intensity
255 and guiding the higher photocatalytic activity under areas with shorter wavelengths.

256 (3) N-doped TiO₂ asphalt road material had a complicated photocatalytic mechanism.

257 By following the experimental results of the present study, we found that NO₂
258 decontamination ability was lower on the N-doped TiO₂ asphalt road material under light
259 irradiation. It has been shown that NO₂ was created in the photocatalytic purification process to
260 decrease NO₂decontamination ability. This may be explained by a tentative mechanism that is
261 proposed to explain photocatalytic oxidation of NO_x under visible light on the N-doped TiO₂
262 asphalt road surface, which is shown in Figure. 10.

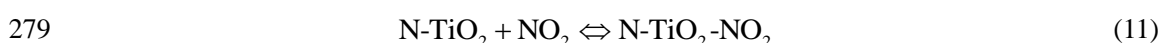
263 It is widely recognized that photocatalytic oxidation can be divided into 3 core stages: first

264 the transfer of contaminants from bulk to the surface; second the adsorption on the catalyst surface
 265 and formation of reactive ions ; finally, degradation by the ions formed on the surface (Chuck et
 266 al.2 013). Based on Figure 10, a possible photocatalytic NO_x oxidation mechanism was proposed
 267 using equations (7)-(18).

268 N doping can build impurity states below the bottom of the conduction band of TiO₂ asphalt
 269 material, causing visible TiO₂ asphalt material to be activated by visible light (Hongqi et al.2011).
 270 N-doped TiO₂ asphalt road material was irradiated by appropriate light and energy, creating a hole
 271 and electron pair in the N-doped TiO₂ lattice, shown in equation (7).



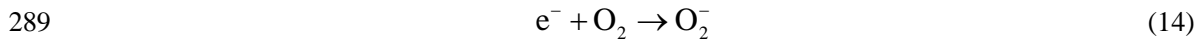
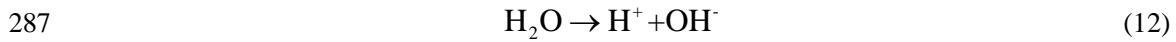
273 During adsorption of the reactants onto the N-doped TiO₂ asphalt road material, the
 274 photogenerated hole in the conduction band will absorb water, oxygen, nitric oxide, and
 275 nitrogen dioxide in the air as described in equations (8) - (11).



280 In our previous work (Meng et al.2011), we found that adsorbed H₂O on the N-doped TiO₂
 281 leads to the formation of a highly hydroxylated surface and also gives off hydrogen ions (H⁺) and
 282 hydroxide ions (OH⁻) by its dissociation. Then, H⁺ reacts with OH⁻ to generate • OH.

283 Additionally, the photoinduced electron reacts with O₂, forming the superoxide anion (O₂⁻)
 284 and O₂⁻ forms HO₂ • radicals with traces of water. Lastly, nitrogen species (NO, NO₂) in the air can
 285 be easily photocatalytically oxidized leading to HNO₃ by HO₂ • radicals on the N-doped TiO₂

286 asphalt road surface. The reaction is illustrated in equations (12) to (18).



294 Durability Analysis

295 Figure. 11 shows the downward trend, over consecutive months, of the NO_x decontamination
296 ability on the N-doped TiO₂ asphalt road. In order to predict the durability of the N-doped TiO₂
297 asphalt road, we hypothesized that the N-doped TiO₂ asphalt road will actively degrade when the
298 NO_x decontamination rate is less 5%. An exponential regression model was used with the
299 observed data that was obtained in the field test (see Figure 11). The model was
300 $y=32.01e^{(-0.145x)}$, with 95% confidence. Results from the model showed that active degradation
301 of the asphalt pavement lasted for a period of about 13 months. The photocatalytic efficiency
302 defeat was due to the wear from traffic and the rain wash. Wear and wash simulation tests were
303 completed in order to analyze these reasons.

304 In the wear simulation test, as seen in table 2, the data showed s decrease in NO_x
305 decontamination ability after wearing. However, the decrease was small under a certain scope,
306 such as in 8000 cycles where the wheel applied a load of 600 N for every cycle. But when the
307 cycle increased (exceeding 8000 cycles), the degree of decrease in the NO_x decontamination

308 ability increased. This had two possible causes: (1) the samples kept higher NO_x removal
309 efficiencies after wear, and, (2) N-doped TiO₂ was retained on the asphalt road surface and interior
310 after wearing, which may be proven by figure 12. This may be attributed to the research team's
311 use of infiltration liquid with N-doped TiO₂ and the permeability loading method. The infiltration
312 liquid had a special lipophilic penetration ability. When the infiltration liquid is sprayed on the
313 road surface, the nano-material (N-doped TiO₂) can be guaranteed to gradually infiltrate the road
314 surface under the action of the penetrating agent molecular power. Subsequently, with the growth
315 of the concentration of the asphalt pavement surface infiltration liquid and the dual influences of
316 the concentration gradient and porous open graded pavement, N-doped TiO₂ penetrates along the
317 open graded asphalt pavement pore to the core under the action of capillary force and gravity.
318 During the penetration process, when the N-doped TiO₂ molecules are near the asphalt mixture
319 solid surface, N-doped TiO₂ molecules can adsorb on the solid surface in order to achieve the load.
320 This is because of the electric dipole moment and is possible because of the help of the Van Der
321 Waals force. However, when the cycle increases, the loss of weight in the samples also increases.
322 Surface wearing and particle loss may be associated with the loss of N-doped TiO₂ particles,
323 which is shown in figure 13. NO_x decontamination ability decreases as the cycles increase.

324 Table 2 presents the average NO_x decontamination ability for both the original and the
325 washed samples. The table shows that washing the samples results in reduction in the NO_x
326 removal efficiency and this decline was aggravated with time. This indicates time dependency,
327 which will result in a decrease of the NO_x removal efficiency. There are many reasons for this.
328 First, the decrease can be clarified by referencing the NO_x purification mechanisms found in
329 section 3.2 of this paper. HNO₃ should be speedily produced and accumulated on the top of the

330 N-doped TiO₂ asphalt road surface, and this could inhibit the photocatalytic reactions by building
331 a physical fence. Next, regeneration of the purification ability has proven that washing is a better
332 way to keep the NO_x decontamination ability for N-doped TiO₂ asphalt road material. During
333 washing, the HNO₃ was easily removed from the catalyst surface (as indirect measurement results);
334 it can be argued this may contribute to catalyst regeneration. Water can also, through rehydration,
335 replenish the consumed hydroxyl radicals; therefore, it is able to maintain the photocatalyst
336 activity (Meng et al.2011). However, the continuing decrease of the NO_x removal efficiency also
337 indicated that washing did not totally recover the active N-doped TiO₂ asphalt road material. That
338 may be due to the adsorption of indissolvable materials, such as lipids, on the photocatalyst
339 receptor sites of N-doped TiO₂ asphalt road material. Adsorption of NO_x occurred on the N-doped
340 TiO₂ asphalt road.

341 Summary and future work

342 N-doped TiO₂ powders were successfully prepared by sol–gel methods with urea. The
343 modified procedures did not change the crystalline structure or the morphology of the N-doped
344 TiO₂ as compared with initial sol–gel TiO₂. TEM analysis revealed that N-doped TiO₂ powders
345 could be well dispersed in asphalt penetrants. Based on the penetrant, N-doped TiO₂ asphalt road
346 materials were successfully prepared using spray methods.

347 Meanwhile, the N-doped TiO₂ asphalt road materials presented higher activity on NO_x
348 removal than pure TiO₂ asphalt road materials under the irradiation of visible light. The outcome
349 was ascribed to the photocatalytic mechanism. As described by this mechanism, the nitrogen
350 species onto The iO₂ interfaces decreased the absorption band gap energy in the visible light and
351 hindered the electron hole recombination, which helped to improve oxidation of nitrogen oxides.

352 The durability of N-doped TiO₂ asphalt road materials was evaluated through field and
353 simulation testing. Results suggested that the durability of N-doped TiO₂ asphalt road materials
354 spanned a period of approximately 13 months. The results demonstrated that the TiO₂ nitrogen
355 doping approach would provide a worthy channel for photocatalytic asphalt road materials of
356 highly visible light induced photocatalytic activity for the practical decontamination NO_x
357 application in the medium-term.

358 Because the application of N-doped TiO₂ asphalt road materials in demonstrating vehicle
359 emissions is still a relatively new field of study, more research should be conducted prior to field
360 application. Our research team plans to evaluate the potential pollution of nitrates created by the
361 photocatalytic processing in land through plant experiments. We will also attempt to build an
362 evaluation system for N-doped TiO₂ asphalt road materials application for demonstrating vehicle
363 emissions.

364 Acknowledgments

365 The authors gratefully acknowledge the funding support by the National Natural Science
366 Foundation of China (Grant No. 31470611, 51378096), Research Fund for the Doctoral Program
367 of Higher Education of China (Grant No. 20120062120011) ,the Natural Science Foundation of
368 Heilongjiang Province (Grant No. E2015055) and the Fundamental Research Funds for the
369 Central Universities (Grant No. 2572014CB16), respectively.

370

371 **References**

372 Giacomo Barolo, Stefano Livraghi, Mario Chiesa, Maria Cristina Paganini, and Elio Giamello.
373 (2012). "Mechanism of the Photoactivity under Visible Light of N-Doped Titanium

374 Dioxide. Charge Carriers Migration in Irradiated N-TiO₂ Investigated by Electron
375 Paramagnetic Resonance. ” The Journal of Physical Chemistry C 116:20887–20894.

376 Hao-Hong Chen, Fang Lei, Jing-Tai Zhao, Ying Shi ,Jian-Jun Xie. (2013). “Preparation and
377 photovoltaic properties of N-doped TiO₂ nanocrystals in vacuum.” Journal of Materials
378 Research 28:468-47.

379 Meng Chen, Jiang-Wei Chu. (2011). “NO_x photocatalytic degradation on active concrete road
380 surface d from experiment to real-scale application.” Journal of Cleaner Production 19:
381 1266-1272.

382 Meng Chen, Li sheng Jin, Yanhua Liu, Xiurong Guo, Jiangwei Chu. (2014). “Decomposition of
383 NO in automobile exhaust by plasma-photocatalysis synergy.” Environmental Science and
384 Pollution Research 21:1242–1247.

385 Meng Chen, Yan hua Liu. (2010). “NO_x removal from vehicle emissions by functionality surface
386 of asphalt road.” Journal of Hazardous Materials 174:375–379.

387 Poon CS, Cheung E (2006). “NO removal efficiency of photocatalytic paving blocks prepared
388 with recycled materials.” Construction and Building Materials 21: 1746–53.

389 Husken G, Hunger M, Brouwers H. (2007). “Comparative study on cementitious products
390 containing titanium dioxide as photo-catalyst. ” In: Baglioni P, Cassar L, eds. RILEM Int.
391 Symp. On Photocatalysis. Environment and Construction Materials. Italy 147–54.

392 G.L.Guerrini, E.Peccati. (2007). “Photocatalytic cementitious roads for depollution, in: P.Baglioni,
393 L. Cassar (Eds.), Proceedings international RILEM symposium on photocatalysis.”
394 Environment and construction materials-TDP 2007, RILEM Publications, Bagneux
395 187–194.

396 Ishihara, H., Koga, H., Kitaoka, T., Wariishi, H., Tomoda, A., Suzuki, R. (2010). "Paper-structured
397 catalyst for catalytic NO_x removal from combustion exhaust gas." *Chemical Engineering*
398 *Journal* 65: 208–213.

399 Marwa Hassan, Louay N. Mohammad, Somayeh Asadi. (2013). "Sustainable Photocatalytic
400 Asphalt Pavements for Mitigation of Nitrogen Oxide and Sulfur Dioxide Vehicle
401 Emissions." *Journal of Materials in Civil Engineering* 3:365-371.

402 Chun-Hung Huanga, I-Kai Wanga, Yu-Ming Linb, Yao-Hsuan Tsengc, Chun-Mei Lud. (2010).
403 "Visible light photocatalytic degradation of nitric oxides on PtOx-modified TiO₂ via
404 sol-gel and impregnation method." *Journal of Molecular Catalysis A: Chemical*
405 316:163–170.

406 Chun-Hung Huang, Yu-Ming Lin, I-Kai Wang, and Chun-Mei Lu. (2012). "Photocatalytic Activity
407 and Characterization of Carbon-Modified Titania for Visible-Light-Active
408 Photodegradation of Nitrogen Oxides." *International Journal of Photoenergy* 2012: 1-13.

409 Venturini, L., and Bacchi, M. (2009). "Research, design, and development of a photocatalytic
410 asphalt pavement." *Proc., 2nd Int. Conf. on Environmentally Friendly Roads, Road and*
411 *Bridge Research Institute, Warsaw, Poland* 1–16.

412 Marwa M.Hassan, Heather Dylla, Louay N.Mohammad, Tyson Rupnow. (2010). "Evaluation of
413 the durability of titanium dioxide photocatalyst coating for concrete pavement."
414 *Construction and Building Materials* 24:1456–1461.

415 Todorova,N, T.Vaimakis, D. Petrakis, S. Hishita, N. Boukos, T. Giannakopoulou, M. Giannouri,S.
416 Antiohos, D. Papageorgiou, E. Chaniotakis, C. Trapalis. (2013). "N and N,S-doped TiO₂
417 photocatalysts and their activity in NO_x oxidation." *Catalysis Today* 209:41–46.

418 Tarek Mohamed Naser, Isao Kanda, Toshimasa Ohara, Kazuhiko Sakamoto, Shinji Kobayashi,
419 Hiroshi Nitta, Taro Nataami. (2009). "Analysis of traffic-related NO_x and EC
420 concentrations at various distances from major roads in Japan." Atmospheric Environment
421 43: 2379–2390.

422 David Osborn, Marwa Hassan, Somayeh Asadi, John R. White. (2014). "Durability Quantification
423 of TiO₂ Surface Coating on Concrete and Asphalt Pavements." Journal of Materials in
424 Civil Engineering 26:331-337.

425 Gagoa.R, A. Redondo-Cubero b, M. Vinnichenkoc, J. Lehmannc, F. Munnikc, F.J. Palomares.
426 (2012). "Spectroscopic evidence of NO_x formation and band-gap narrowing in N-doped
427 TiO₂ films grown by pulsed magnetron sputtering." Materials Chemistry and Physics
428 136:729-736.

429 Shinri Sato. (1986). "Photocatalytic activity of NO_x-doped TiO₂ in the visible light region."
430 Chemical Physics Letters 123:126-128.

431 Kumar.S.C, L.G. Devi. (2011). "Review on modified TiO₂ photocatalysis under UV/visible light:
432 selected results and related mechanisms on interfacial charge carrier transfer dynamics."
433 Journal of Physical Chemistry A 115:13211–13241.

434 Hongqi Sun, Ruh Ullah, Siewhui Chong, Hua Ming Ang, Moses O. Tadé, Shaobin Wang. (2011).
435 "Room-light-induced indoor air purification using an efficient Pt/N-TiO₂ photocatalyst."
436 Applied Catalysis B: Environmental 108–109:127–133.

437 Yao-Hsuan Tseng, Chien-Hung Kuo. (2011). "Photocatalytic degradation of dye and NO_x using
438 visible-light-responsive carbon-containing TiO₂." Catalysis Today 174:114–120.

439 Yu.Y, J. C. Yu, J. G. Yu. (2005). "Enhancement of photocatalytic activity of mesoporous TiO₂ by

440 using carbon nanotubes.” *Applied Catalysis A*289: 186–196.

441 Shu Yin, Bin Liu, Peilin Zhang, Takeshi Morikawa, Ken-ichi Yamanaka, and Tsugio Sato. (2008).

442 “Photocatalytic Oxidation of NO_x under Visible LED Light Irradiation over

443 Nitrogen-Doped Titania Particles with Iron or Platinum Loading.” *Journal of Physical*

444 *Chemistry. C* 112: 12425–12431.

445 Shu Yin, Hiroshi Yamaki, Qiwu Zhang, Masakazu Komatsu, Jinshu Wang, Qing Tang, Fumio Saito,

446 Tsugio Sato. (2004). “Mechanochemical synthesis of nitrogen-doped titania and its visible

447 light induced NO_x destruction ability.” *Solid State Ionics* 172:205–209.

448 Chuck W.F. Yu, Jeong Tai Kim. (2013). “Photocatalytic Oxidation for Maintenance of Indoor

449 Environmental Quality.” *Indoor and Built Environment* 22: 139-51.

450

451

452

453

454

455

456

457

Table 1 parameter nomenclature

Parameter	Meaning
$NO_{conversion}$ (%)	effective purifying rate of NO
$NO_{2conversion}$ (%)	effective purifying rate of NO ₂
$NO_{xconversion}$ (%)	effective purifying rate of NO _x
C_{NOin} (mg/m ³)	the initial steady-state NO concentration (before turn on the light source)
$C_{NO_{2in}}$ (mg/m ³)	the initial steady-state NO ₂ concentration (before turn on the light source)
$C_{NO_{xin}}$ (mg/m ³)	the initial steady-state NO _x concentration (before turn on the light source)
$C_{NOlight}$ (mg/m ³)	the NO concentration during irradiation phase
$C_{NO_{2light}}$ (mg/m ³)	the NO ₂ concentration during irradiation phase
$C_{NO_{xlight}}$ (mg/m ³)	the NO _x concentration during irradiation phase
C_{NObin} (mg/m ³)	the initial steady state NO concentration
$C_{NO_{2bin}}$ (mg/m ³)	the initial steady state NO ₂ concentration
$C_{NO_{xbin}}$ (mg/m ³)	the initial steady state NO _x concentration
C_{NOsb} (mg/m ³)	the NO concentration at the end of the blank experiment(without irradiation)
$C_{NO_{2sb}}$ (mg/m ³)	the NO ₂ concentration at the end of the blank experiment(without irradiation)
$C_{NO_{xsb}}$ (mg/m ³)	the NO _x concentration at the end of the blank experiment(without irradiation)

459

460

461

462

463

464

Table 2 Degradation effect of wear and wash

DeNO _x ability	Number of wear (cycle)					Number of wash (time)				
	0	4000	8000	12000	16000	0	2	4	6	8
Direct measurement-purification rate (%)	36.4	34.8	32.1	28.1	22.3	36.4	34.2	32.8	29.3	24.6
Indirect measurement- nitrate concentrations in the sample (mg/L)	8.3	8.1	7.2	5.5	3.8	8.3	7.9	7.3	6.1	4.1



Fig 1. Pure TiO₂ and N-doped TiO₂



Fig 2. Asphalt road material sample before spray



Fig 3. N-doped TiO₂ asphalt road material sample

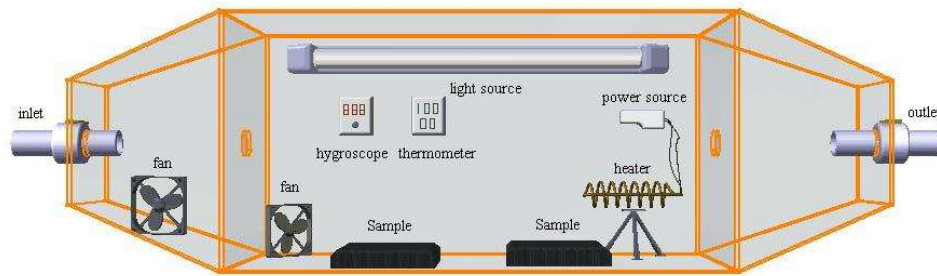


Fig 4. Structure of photoreactor



Fig 5. Spot of field test



Fig 6. Simulation test on vehicular activity effect

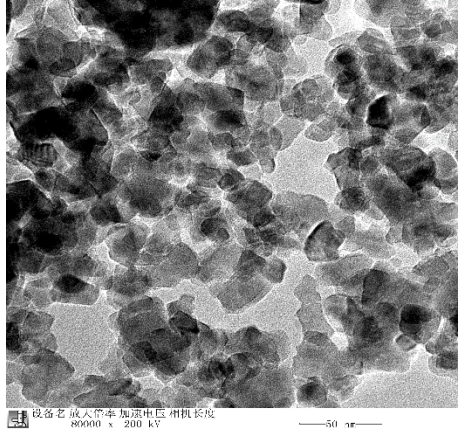


Fig 7. Micrographs of the N-doped TiO₂

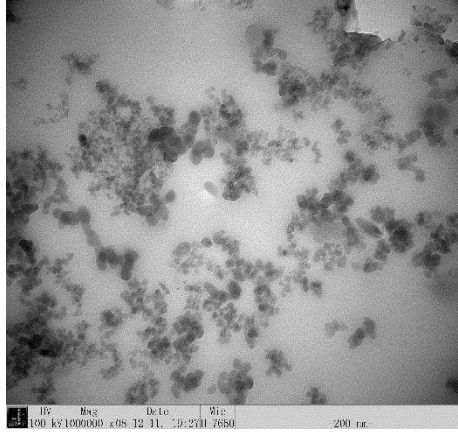


Fig 8. Dispersion effect of N-doped TiO₂ in penetrant

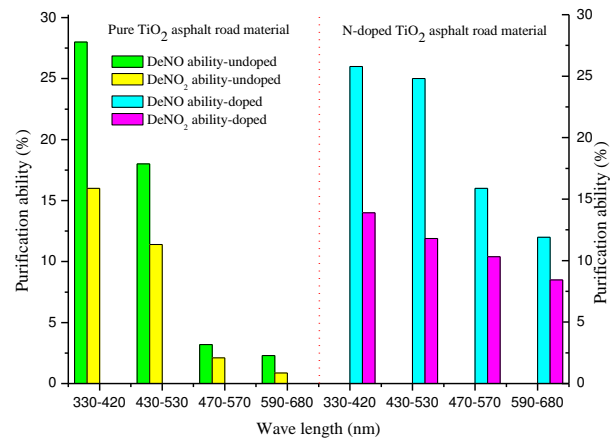


Fig 9 Comparison of the photocatalytic activity of undoped, N-doped TiO₂ asphalt road material under UV and visible light

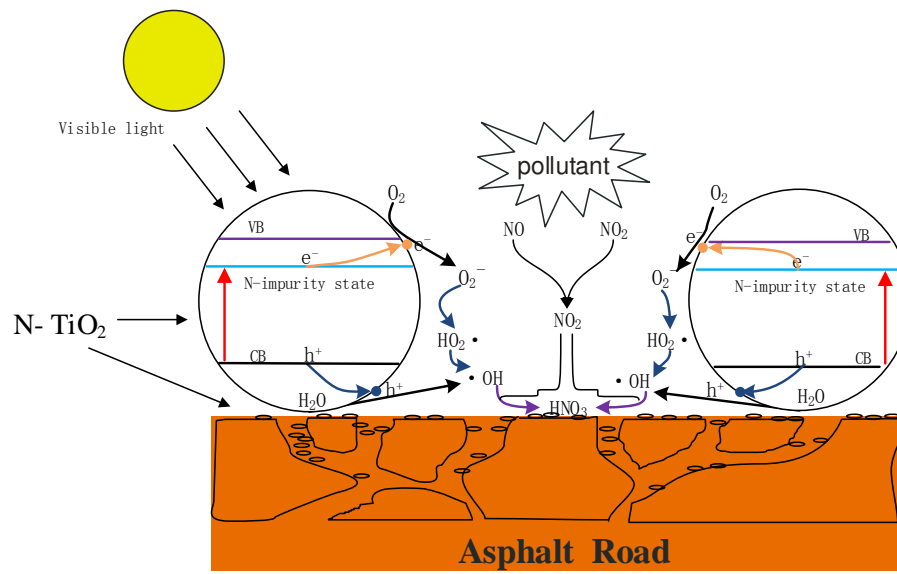


Fig 10. Schematic illustration of photocatalytic process on N-doped TiO₂ asphalt road material under visible light

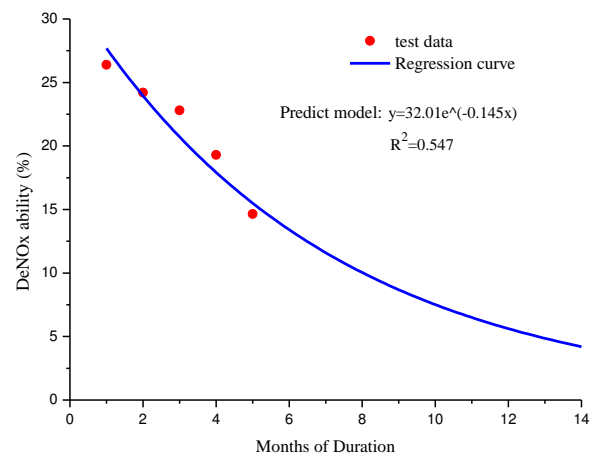


Fig 11 Illustration of durability of N-doped TiO₂ asphalt road

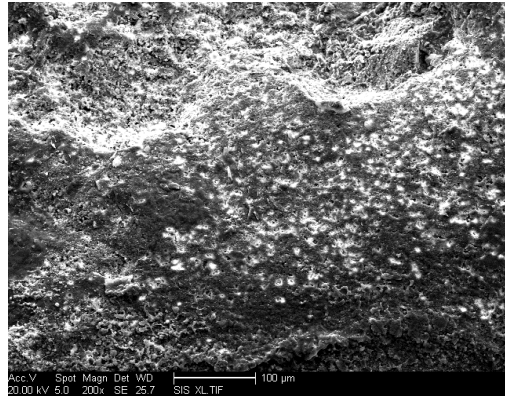


Fig 12 SEM image of road surface after wearing

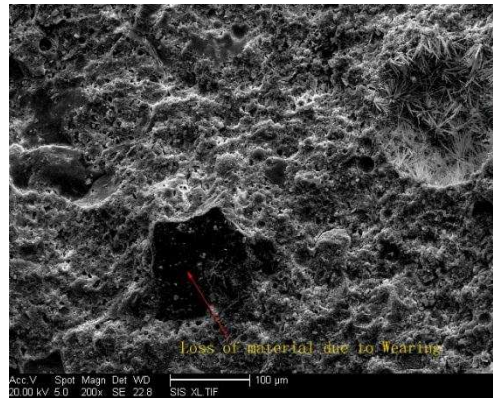


Fig 13 SEM on loss of N-doped TiO_2 due to wearing

Fig 1. Pure TiO₂ and N-doped TiO₂

Fig 2. Asphalt road material sample before spray

Fig 3. N-doped TiO₂ asphalt road material sample

Fig 4. Structure of photoreactor

Fig 5. Spot of field test

Fig 6. Simulation test on vehicular activity effect

Fig 7. Micrographs of the N-doped TiO₂

Fig 8. Dispersion effect of N-doped TiO₂ in penetrant

Fig 9 Comparison of the photocatalytic activity of undoped, N-doped TiO₂ asphalt road material under UV and visible light

Fig 10. Schematic illustration of photocatalytic process on N-doped TiO₂ asphalt road material under visible light

Fig 11 Illustration of durability of N-doped TiO₂ asphalt road

Fig 12 SEM image of road surface after wearing

Fig 13 SEM on loss of N-doped TiO₂ due to wearing